BIOCHEMISTRY
including biophysical chemistry & molecular biology

Accelerated Publication

pubs.acs.org/biochemistry

Dramatic Domain Rearrangements of the Cyanobacterial Orange Carotenoid Protein upon Photoactivation

Haijun Liu,[†,‡] Hao Zhang,[‡,§] Gregory S. Orf,[‡,§] Yue Lu,[‡,§] Jing Jiang,[‡] Jeremy D. King,[†,‡] Nathan R. Wolf,[‡,§] Michael L. Gross,[‡,§] and Robert E. Blankenship*[,†,‡,§]

[†]Department of Biology, [‡]Photosynthetic Antenna Research Center (PARC), and [§]Department of Chemistry, Washington University in St. Louis, St. Louis, Missouri 63130, United Sates

ABSTRACT: Photosynthetic cyanobacteria make important contributions to global carbon and nitrogen budgets. A protein known as the orange carotenoid protein (OCP) protects the photosynthetic apparatus from damage by dissipating excess energy absorbed by the phycobilisome, the major light-harvesting complex in many cyanobacteria. OCP binds one carotenoid pigment, but the color of this pigment depends on conditions. It is orange in the dark and red when exposed to light. We modified the orange and red forms of OCP by using isotopically coded cross-linking agents and then analyzed the structural features by using liquid chromatography and tandem mass spectrometry. Unequivocal cross-linking pairs uniquely detected in red OCP indicate that, upon photoactivation, the OCP N-terminal domain (NTD) and C-terminal domain (CTD) reorient relative to each other. Our data also indicate that the intrinsically unstructured loop connecting the NTD and CTD not only is involved in the interaction between the two domains in orange OCP but also, together with the N-terminal extension, provides a structural buffer system facilitating an intramolecular breathing motion of the OCP, thus helping conversion back and forth from the orange to red form during the OCP photocycle. These results have important implications for understanding the molecular mechanism of action of cyanobacterial photoprotection.

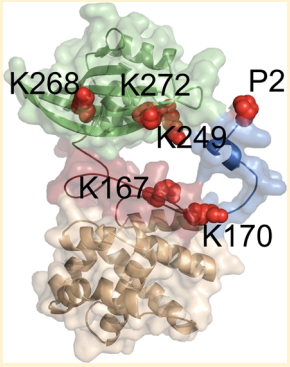

Photosynthesis converts solar energy to chemical energy in plants, algae, cyanobacteria, and other phototrophic bacteria.[1] In this process, light energy initially absorbed by light-harvesting antenna complexes (LHC) is delivered to the reaction centers (RCs) where photochemistry takes place.[2,3] Energy currency (ATP) and reducing power (NADPH) generated from light-driven electron transport are then used for carbon fixation in a light-independent manner. Solar energy conversion rates in photosynthetic systems, however, are not constant. Instead, cellular energy requirements vary depending on cellular developmental stage, growth condition, carbon fixation capacity, and others. If solar energy absorbed by LHCs exceeds the photochemical conversion capacity and cellular energy requirements, the excess energy has to be safely dissipated as heat in a process called nonphotochemical quenching (NPQ).[4] NPQ is one of multiple strategies that cells have evolved to regulate the energy arriving at RCs and to reduce the production of reactive oxygen species that are damaging or lethal if not properly managed. In plants and algae, the thermal dissipation of excitation energy occurs at the membrane-bound chlorophyll antenna of Photosystem II;[5,6] an equivalent photoprotective mechanism in cyanobacteria takes place, however, in the cytosol where the major LHC, known as the phycobilisome (PBS), is located.[7,8]

The orange carotenoid protein (OCP) is a pigment−protein complex with a molecular weight (MW) of 35 kDa[9−11] and is involved in NPQ in many cyanobacteria.[12] The OCP has two structural domains, with an N-terminal domain (NTD) consisting of mainly α-helix secondary structure and a C-terminal domain (CTD) consisting of two discontinuous four-helix bundles and a mixed α/β structure. A 4-keto carotenoid (3′-hydroxyechininone) spans both domains and is almost entirely buried by the protein matrix. In addition to this connection, the NTD and CTD interact through two other distinct regions. The first 19 amino acids of the NTD, which are comprised of a short α-helix (αA) and an unstructured loop, extend away from the N-terminal α-helical bundle and interact with the solvent-exposed surface of the C-terminal domain β-sheet. The second interaction is at the interface of the NTD and CTD, which buries 1722 Å^2 of surface area.[13] Upon light illumination, OCP (orange OCP, OCP^o) undergoes conversion to a red form (OCP^r) and consequently becomes able to bind to the PBS, allowing the excitation energy dissipation of the latter via energy transfer to the carotenoid molecule of OCP, and thereby preventing oxidative damage under high-light conditions.

The NTD and CTD likely have discrete functions during the OCP photocycle. Mass spectrometry-based carboxyl group footprinting indicates that the N-terminal extension (NTE), containing αA (the first α-helix from N-terminus of OCP), plays a key role in the structural rearrangements of OCP during photoactivation.[14,15] Although the NTE is located on and associated with the outside of the β-sheet core in the CTD of OCP under dark conditions, light-induced changes in the

Received: January 8, 2016
Published: February 5, 2016

DOI: 10.1021/acs.biochem.6b00013
Biochemistry 2016, 55, 1003−1009

pigment molecule disrupt this interaction, allowing global tertiary structural changes and favoring complete domain dissociation of the NTD and CTD.[13] It was suggested that the NTD's newly exposed surface, which is normally buried in the interface of the NTD and CTD in OCP^o, is involved in the association with PBS.[16] The restoration of light harvesting by PBS to the RCs represents the reverse process. Fluorescence recovery is facilitated by the fluorescence recovery protein (FRP),[17] which is thought to interact with the OCP CTD through a domain that is not exposed until OCP is fully activated.[14,18] Even though structural and functional models of the OCP have been proposed,[15,16,19−24] many questions regarding the details of the mechanism and the associated protein dynamics in the OCP photocycle remain unanswered.

In this study, we used isotopically coded chemical cross-linking reactions and FPLC separation and mass spectrometry to investigate the reorientation of the NTD and CTD upon OCP photoactivation. We report here that chemical cross-linking can lock in and thereby track structural features of OCP^r. The results indicate that the NTD and CTD are juxtaposed in a way that the NTE, loop J−K (the linker domain between the CTD and NTD), and the surface of the β-sheet core of CTD are in structural proximity, presenting a fully exposed interface of the NTD for PBS binding and excitation energy quenching. The distance constraints are used for generating a molecular model of OCP^r.

MATERIALS AND METHODS

Growth of *Synechocystis* sp. PCC 6803 and OCP Isolation. The cell growth and the OCP isolation were described elsewhere.[21,25]

Chemical Cross-Linking. OCP was resuspended at 0.1 mg/mL in 20 mM MOPS buffer (pH 7.0). NHS-ester-based chemical cross-linking (BS^3, DSS, Thermo Scientific, Rockford, IL) was performed according to the manufacturer's protocol followed by desalting by using Zeba spin columns (Thermo Scientific). Isotopically coded cross-linkers (BS^3-H_{12}/D_{12} and DSS-H_{12}/D_{12}) were purchased from Creative Molecules, Inc. (http://www.creativemolecules.com/).

Protein Analysis and FPLC Isolation of Monomeric, Cross-Linked OCP. Protein electrophoresis was performed as described previously[26] unless otherwise indicated. A Superdex 75 10/300GL column was used for separating the cross-linked products of OCP^o and OCP^r.

Sample Digestion, LC−MS/MS, and Data Processing. Cross-linked OCP samples were precipitated by acetone precipitation and then digested with LysC and trypsin by following the previously published method.[27] In brief, protein pellets were dissolved in an 8 M urea solution (20 μL) followed by incubation with tris(2-carboxyethyl)phosphine (2.5 mM) at 37 °C for 30 min and iodoacetamide (5 mM) for 30 min at room temperature. A LysC stock solution (0.5 μg/μL, 2 μL for each sample) was added to initiate the digestion at 37 °C. After LysC digestion for 2 h, the protein solution (8 M urea) was diluted (1 M urea) by adding Tris buffer (100 mM). The protein solution was further incubated with trypsin overnight at 37 °C. The digestion was quenched by adding 0.1% formic acid.

An aliquot (5 μL, 1 pmol of protein digest) was loaded onto a trap column (180 μm × 2 cm, C18 Symmetry, 5 μm, 100 Å, Waters, Milford, MA) using solvent A (water with 0.1% formic acid). Peptides were eluted from a reverse phase C18 column (BEH 130, 75 μm × 150 mm, Waters) by increasing the fraction of solvent B (80% acetonitrile, 20% water, and 0.1% formic acid). The gradient was supplied by a Dionex UltiMate 3000 instrument (Thermo Scientific, Inc., Sunnyvale, CA) and run from 2 to 40% solvent B over 90 min and then to 95% solvent B for 10 min at a rate of 250 nL/min followed by a 5 min re-equilibration step with 98% solvent A. The flow was directed by a Nanospray Flex source into a Q Exactive Plus mass spectrometer (Thermo-Scientific, San Jose, CA) with a spray voltage of 1.8 kV and a capillary temperature of 300 °C. The Q Exactive Plus spectrometer was operated in standard data-dependent acquisition mode controlled by Xcalibur version 3.0.63. Peptide mass spectra (m/z range of 380−1500) were acquired at a high mass resolving power (70000 for ions at m/z 200) with the Fourier transform (FT) mass spectrometer. The Q Exactive plus spectrometer was externally calibrated using a standard mixture of caffeine, MRFA, and Ultramark 1621. The mass calibration was checked and repeated before the LC−MS experiments to optimize mass measurement accuracy. In the data-dependent mode, the 10 most abundant multiply charged ions with a minimal intensity of 5×10^4 counts were subjected to high-energy collision-induced dissociation (HCD). Precursor activation in HCD was performed with an isolation width of m/z 1.5 and a normalized collision energy of 27%.

The raw data were directly loaded into PEAKS (version 7.0, Bioinformatics Solution Inc., Waterloo, ON) for protein identification. The raw data were converted to a .mgf file by ProteoWizard.[28,29] The compact data files (raw data and .mgf files) were submitted to ProteinProspector.[30,31] The same data were searched twice with H_{12} and D_{12} cross-linkers separately. The score cutoff was 40 in the identification of cross-linked peptides.

Protein Modeling. After collection of cross-linking data, a feasible model for photoactivated OCP^r was sought by loading the OCP^o crystal structure into PyMol[32] (Schrödinger, LLC). An x−y plane that bisects, and is perpendicular to, the long axis of the carotenoid cofactor was defined. This x−y plane, therefore, occupies the boundary between the NTD and CTD. Eight models were then generated in which the CTD is allowed to flip over, as if on a hinge, at 45° increments along the plane around the diameter of the protein, so that the interface of the NTD, which usually interacts with the CTD in OCP^o, was totally exposed. Cross-linking pairs observed in our experiments were then used as structural constraints to eliminate unfavorable orientations of the CTD relative to the NTD. Minimizing the spatial conflicts between each cross-linking pair from our experiments led to a single acceptable model.

After the position of the NTD and the new position of the CTD had been locked, the linker domain (loop J−K, residues 161−196) was left as an unstructured, disoriented loop region. The Modeller version 9.15 environment (https://salilab.org/modeller/)[33,34] was utilized to generate possible structural models for this region. Modeller is generally used for comparative protein modeling with spatial restraints for applications such as homology modeling, but it contains functions for the refinement of existing protein structures. A Loop Refinement Python script was generated using Modeller's "loopmodel" class, which generates low-energy models for a loop region of an existing protein structure without comparative modeling. An example script for this process can be found in the online manual (https://salilab.org/modeller/manual/). In this script, the loopmodel.select_loop_atoms routine was redefined so that refinement of the loop in question did not require a comparative model. The script was written

DOI: 10.1021/acs.biochem.6b00013
Biochemistry 2016, 55, 1003−1009

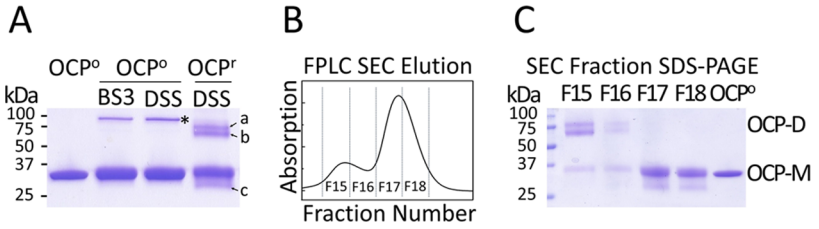

Figure 1. Chemical cross-linking of OCP. (A) SDS−PAGE analysis showing different cross-linking products of OCP° and OCP^r after Coomassie Brilliant Blue (R-250) staining: lane 1, OCP°, control; lanes 2 and 3, OCP° treated with BS^3 and DSS, respectively, *78 kDa; lane 4, OCP^r treated with DSS, bands a (76 kDa), b (70 kDa), and c (28 kDa). (B) Typical FPLC SEC elution profile (partial) of cross-linked species of OCP^r. Fractions (F) are labeled. (C) SDS−PAGE analysis of panel B. The locations of OCP-M (monomer) and OCP-D (dimer) are indicated.

such that the NTD and CTD would remain spatially static, with loop refinement performed on just residues 161−196. One hundred models were generated, and the five models with the lowest discrete optimized protein energy (DOPE) scores were assessed.[33] Of the five, the single model that best satisfied the spatial restraints imposed by chemical cross-linking results was retained. This final model, incorporating the new CTD position and refined loop J−K, was chosen as our preferred model for OCP^r.

RESULTS AND DISCUSSION

Chemical cross-linking in combination with mass spectrometry has become a widely used tool in structural proteomics for studying protein−protein interactions and determining low-resolution structures and topology.[35,36] This method can additionally provide important supplementary information concerning the structural organization and identification of conformational changes occurring during enzymatic reactions. Modification of OCP° and OCP^r by a chemical cross-linker [BS^3, DSS (non-isotopically coded)] resulted in different cross-linked species (Figure 1A). In the absence of a cross-linker, OCP migrated as a single band at 35 kDa via SDS−PAGE. Treatment with a NHS-ester-type cross-linker (i.e., BS^3 or DSS of OCP°) resulted in the formation of a major product with a MW of approximately 78 kDa as well as a major band with a MW of 35 kDa (Figure 1A, lanes 2 and 3). According to these values and using unmodified OCP as a reference (Figure 1A, lane 1), we suggest that they correspond to cross-linked, dimerized OCP and cross-linked OCP monomer, respectively. In contrast, treatment of OCP^r resulted in a more complex protein gel pattern (Figure 1A, lane 4): two bands appeared corresponding to proteins with MWs of approximately 76 kDa (band a) and 70 kDa (band b), respectively. A dense band for a 35 kDa monomer and a diffused band corresponding to a 28 kDa band (band c) were also significant. We suggest that the 76 and 70 kDa bands represent the cross-linked OCP dimer with gel migration behavior altered by the chemical modification introduced by chemical cross-linking (e.g., altered MW compared to that of the unmodified protein, altered overall polypeptide shape that affects the gel migration mobility in the electrical field). The 28 kDa band may represent a cross-linked, monomeric OCP, similar to the major 35 kDa band (cross-linking-induced gel migration variations are documented in previous publications[37−39]).

In this study, we were particularly interested in the intramolecular structural changes of OCP upon photoactivation as could be revealed by comparing the cross-linked, monomeric OCP^r to OCP° (Figure 1). The oligomerization state of OCP is controversial according to various analytical perspectives.[11,13,21,40] It seems that dimerization occurs at higher protein concentrations.[13] Whether OCP *in vivo* exists as a monomer or dimer, however, is not certain. We used size-exclusion chromatography (SEC) to purify cross-linked, monomeric OCP protein products after chemical cross-linking. A typical elution profile of OCP^r treated with DSS H_{12}/D_{12} is shown (Figure 1B). The two elution peaks in the chromatogram correspond to OCP dimer and monomer as assigned by comparison to protein standards. To determine if SEC is effective at separating OCP dimer and OCP monomer, different fractions were collected and subjected to further biochemical characterization. In brief, the resulting gel analysis (Figure 1C) indicates that fraction 15 (F15) and F16 contain mostly cross-linked, dimeric OCP with significantly less 35 kDa OCP monomer (Figure 1A, lane 4, and Figure 1C, F15). Remarkably, both F17 and F18 show the major, monomeric 35 and 28 kDa bands, whereas dimeric OCP is not visible (Figure 1C). It should be noted that chemically cross-linked, monomeric OCP^r becomes locked in its red form, failing to convert back to its orange form (data not shown) upon dark relaxation, indicating the red-to-orange conversion pathway is blocked by chemical modification. Similarly, cross-linked, monomeric OCP° is unable to convert to OCP^r.

Chemical cross-linking covalently joins amino acid pairs found in the proximity of each other in a protein or a protein complex.[41−43] After more than a decade of method development, multiple mature platforms of cross-linked species identification have become available.[42,44,45] To determine the locations of intramolecular cross-links of OCP° and OCP^r, purified monomeric OCP° and OCP^r samples were subjected to direct trypsin digestion in solution and the resulting peptides were submitted to extraction and LC−MS/MS analysis (Figure 2A shows the intramolecular cross-links in OCP° and OCP^r).

A consensus that local and global structural changes take place in OCP upon photoactivation has been reached.[11,13,14,21,46] Compared to its red form, OCP° is more compact. In practice, the outcome of protein cross-linking reactions is affected by solvent accessibility and distance between two functional groups. In our experiments, we detected many monolinks that account for peptides that are modified once by the cross-linker but are not linked to a second peptide because a second functional group to complete the cross-link reaction is not readily available. We detected one cross-linked pair in OCP° [i.e., K^{249}−K^{272} (Figure 2B,C)]. K^{249} and K^{272} are located in β2 and β3, respectively, of the OCP crystal structure.[11] This result is consistent with the arm span of 12 Å, which determines the cross-linking capability of DSS. The measured Euclidean Cα−Cα distance in the crystal structure of OCP° between K^{249} and K^{272} is 8.6 Å (Figure 2B, PDB entry 4XB5), and the distance of two primary amines in this pair is 13.0 Å. Also listed is the SAS (solvent accessible surface)

DOI: 10.1021/acs.biochem.6b00013
Biochemistry 2016, 55, 1003−1009

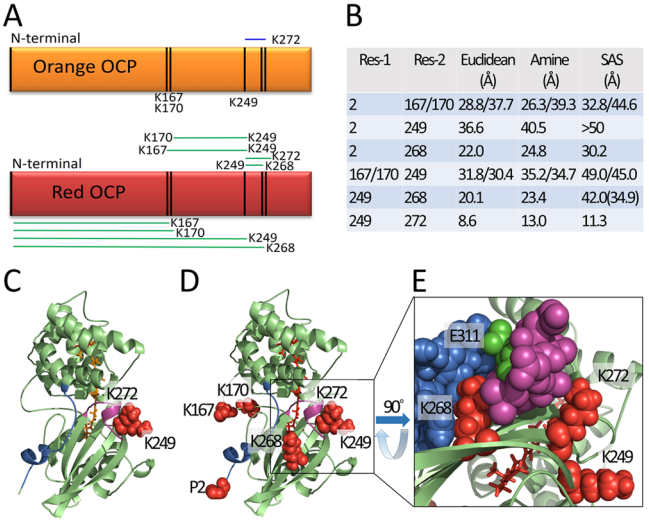

Res-1	Res-2	Euclidean (Å)	Amine (Å)	SAS (Å)
2	167/170	28.8/37.7	26.3/39.3	32.8/44.6
2	249	36.6	40.5	>50
2	268	22.0	24.8	30.2
167/170	249	31.8/30.4	35.2/34.7	49.0/45.0
249	268	20.1	23.4	42.0(34.9)
249	272	8.6	13.0	11.3

Figure 2. Identification of intraprotein cross-links by using LC–MS/MS. (A) Cartoon representation of chemically cross-linked amino acid residues in OCP^{o} and OCP^{r}. (B) Xwalk analysis of cross-linking pairs detected using LC–MS/MS. Listed are the Euclidean Cα–Cα distances between cross-linked lysines determined on the X-ray structure of OCP (PDB entry 4XB5), the side chain amine groups distances, and the SAS distances (see the text for an explanation). (C) K^{249}–K^{272} cross-link in OCP^{o}, NTE (marine), Canthaxanthin (orange, stick), the C-terminal loop (purple), and K^{249} and K^{272} (red, sphere) (PDB entry 4XB5). (D) Amino acid residues involved in cross-linking in OCP^{r}. (E) K^{249}–K^{268} cross-link in OCP^{r}, NTE (marine, sphere), the C-terminal loop (purple, sphere), and E^{311} (green, sphere).

distance, which is 11.3 Å in the case of the K^{249}–K^{272} link. This distance corresponds to the shortest path length between two amino acids, a path that leads through solvent-occupied space without penetrating the protein surface. The K^{249}–K^{272} cross-link was also detected in OCP^{r}, suggesting that the orientation of β2 and β3 upon OCP photoactivation is relatively unaltered (or at least the spatial distance between this pair does not increase to prevent the cross-linking reaction from occurring). This result is consistent with published data.[13]

In addition to this pair, there are seven cross-links uniquely detected in monomeric OCP^{r} (Figure 2B). Among them, three cross-linked pairs have a median Euclidean distance of <30 Å: K^{249}–K^{268} (20.1 Å), P^{2}–K^{268} (22.0 Å), P^{2}–K^{167} (Figure 2B,D). The SAS distance of K^{249}–K^{268} is ~42 Å, and this value decreases to 34.9 Å (Figure 2B,E, pink, spheres) if the C-terminal loop moves away from the β-sheet core as αA does in OCP^{r}.[13,14] It is possible that photoactivation of OCP leads to the dissociation of the C-terminal loop away from the β-sheet core. An increased extent of GEE modification of E^{311} on peptide 311–317 was observed in our mass spectrometry-based protein footprinting analysis.[14] It is more likely, however, that this increase results from αA detachment (blue sphere in Figure 2E) from the β-sheet core rather than the direct detachment of the C-terminal loop. This is consistent with recent HDX exchange results showing no increased solvent accessibility of P^{309} and K^{310}.[13] Therefore, the observed K^{249}–K^{268} cross-link must result from conformational change between β2 and β3 where K^{249} and K^{268} are located, respectively.

Although carboxyl footprinting-based MS[14] and HDX MS[13] have reached a consensus that the NTE dissociates from the β-sheet core of the CTD upon OCP photoactivation, the orientation of this NTE fragment in OCP^{r} remains unclear. It is likely that the NTE becomes very flexible. The P^{2}–K^{268} and P^{2}–K^{167} cross-links may result from the NTE's increased degree of conformational freedom and, thus, provide direct evidence to support such a hypothesis. The OCP^{o} structure has been resolved to the atomic level[11,40] in contrast to that of OCP^{r}, which thus far has not been crystallized. Loop J–K,[11] the NTE, and the C-terminal domain in OCP^{r} may be highly disordered, making crystallization difficult.

We further mapped the four remaining cross-links with Euclidean distances of >30 Å onto the OCP^{o} structure (Figure 2B). The SAS distances of some cross-link pairs are abnormally longer than distances the cross-linking chemistry could afford. For example, although we found that K^{170} is cross-linked to K^{249} by isotopically coded DSS H_{12}/D_{12} (Figure 3), the SAS is

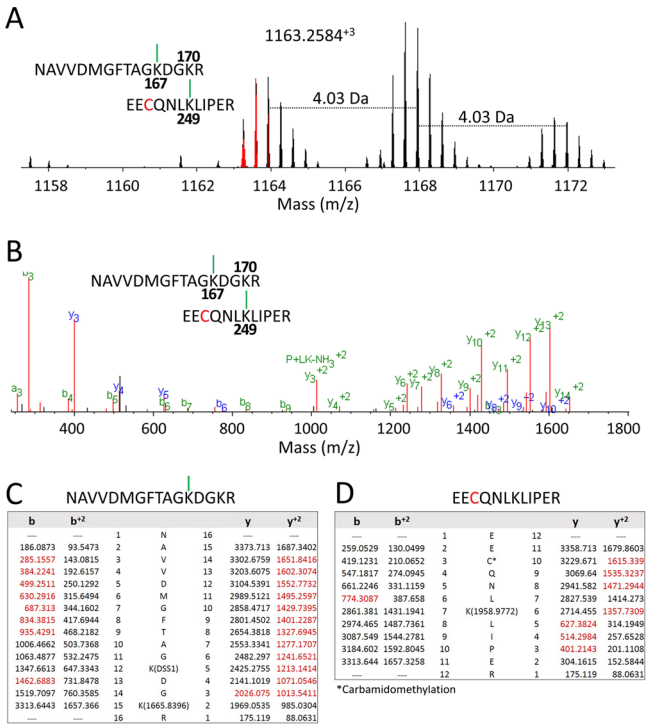

Figure 3. Mass spectra of cross-linked peptides. (A) Mass spectra of peptides NAVVDMGFTAGK^{167}DGK^{170}R and EECQNLK^{249}LIPER. Unique triplet peak with a 1:2:1 ratio and 4.03 Da (z = 3) apart (results from isotopically coded cross-linker DSS-H_{12}/D_{12} that modified two lysine residues, one monolink at K^{167} and one cross-link between K^{170} and K^{249}). (B) Product ion (MS/MS) spectra obtained for cross-linked peptides of panel A. (C and D) Theoretical (black) and identified ions (red) in panel B.

45 Å, almost 4 times longer than the accepted arm span of DSS. The mass spectrum of the cross-linked peptides NAVVDMGFTAGK^{167}DGK^{170}R and EECQNLK^{249}LIPER (Figure 3A) shows that the use of an isotopically coded cross-linker allows unequivocal detection of the cross-linked species. The reaction products of DSS-H_{12}/D_{12} are obvious in the mass spectra and manifest themselves as characteristic doublets of peaks of equal intensity corresponding to light (H_{12}) and heavy (D_{12}) forms of the reagent separated by 12.07573 Da divided by charge state.[47] In this pair of peptides, K^{170} is clearly cross-linked to K^{249} and a monolink is found on K^{167}. Because of the double modification of lysine residues K^{170}–K^{249} (cross-link) and K^{167} (monolink) by two isotopically coded cross-linkers, a characteristic triplet with a 1:2:1 ratio separated by m/z 4.025 (charge of 3) is seen

DOI: 10.1021/acs.biochem.6b00013
Biochemistry 2016, 55, 1003–1009

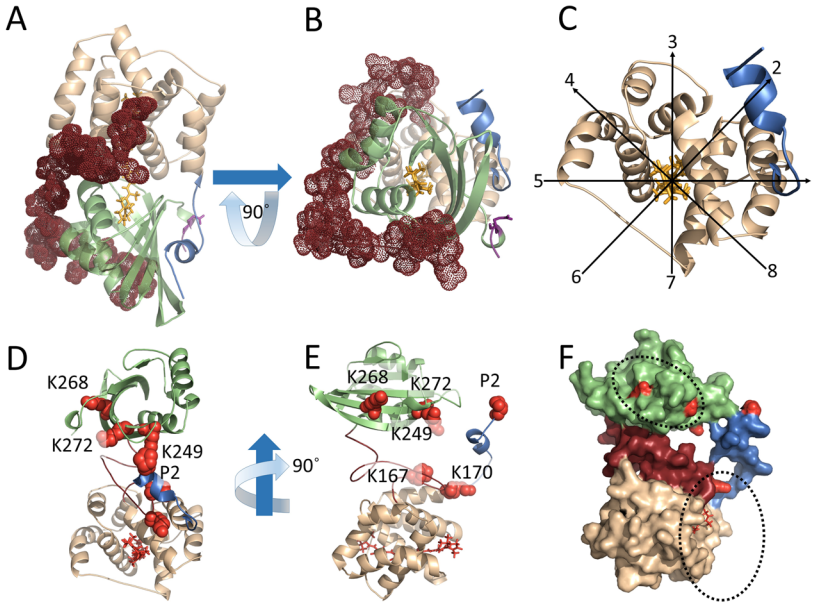

Figure 4. Domain rearrangements of OCP upon light activation. (A) Side view of OCP showing loop J–K (chocolate, joining αJ and αK) and αA (marine) that form a clamp structure holding the CTD (lime) in OCP^o, the NTD (wheat), the C-terminal fragment (purple), and the carotenoid (yellow). (B) Bottom view from the CTD, with loop J–K winding from αJ located in the NTD to αK that is located at the bottom of the CTD, where αA controls the exit of CTD from the opposite side of loop J–K. (C) View of the NTD with CTD and loop J–K removed, based on panel B. (D) Modeled orientation of the NTD and CTD in OCP^r, in which amino acid residues involved in cross-linking are labeled as spheres (red). (E) Side view (90° rotation of panel D). (F) Surface representation of OCP^r, where the circled carotenoid (red stick) region (lower) interacts with the phycobilisome.

as major peaks of the mass spectrum. The accurate modification sites are confirmed by product ion (MS/MS) spectra (Figure 3B–D).

Our present cross-linking data observed for OCP^r add credibility to the hypothesis that OCP undergoes significant conformational changes upon photoactivation, as reached by outcomes from site-directed mutagenesis,[11,15,46] protein footprinting,[13,14] small-angle X-ray scattering (SAXS),[13] and other biophysical techniques.[24] Now the question of how the NTD and CTD reorient relative to each other in OCP^r arises. Even without a crystal structure for OCP^r, we can posit a meaningful model using our cross-linking data as spatial constraints. In the crystal structure of OCP^o, the NTD and CTD are stabilized in two ways: via the major interface between the NTD and CTD and via the minor interface of the NTE and the CTD.[11,40] Additionally, the carotenoid cofactor should also play an important role in stabilizing the NTD and CTD. Another factor that could contribute to the OCP photocycle, in our opinion, is the loop J–K linker region (Figure 4A). This ~25 (depending on species) amino acid residue fragment starts from a short α-helix (αJ) in the NTD and winds its way onto the surface of the CTD and ends at αK of the CTD (Figure 4B). In other words, loop J–K extends like an arm from the interface between the NTD and CTD to the bottom of the latter, holding the CTD from the opposite side of NTE. It is conceivable that the process of OCP photoconverison from orange to red (or vice versa) relates to how the CTD exits from and re-enters the "cradle" formed by loop J–K and the NTE, accompanied by the carotenoid shuttling back and forth into the interior of the NTD.

Our ultimate aim is to generate a model using our cross-linking data as structural constraints.[47] We began by generating eight models in which the CTD of the OCP^o crystal structure is allowed to flip, as if on a hinge, at 45° increments around an x–y plane that bisects normal to the long axis of the carotenoid cofactor. As a result of the CTD flipping, the interface of the NTD that usually interacts with its counterpart of the CTD in OCP^o is totally exposed.[16] Cross-linking pairs that we observed were then used as structural constraints to judge the best orientation of the CTD relative to the NTD. By minimizing the spatial conflicts between each cross-linking pair, we found that the model generated by flipping the CTD outward along axis 3 (Figure 4C) has the fewest spatial conflicts. Then, we used the computer program Modeller to refine and produce a feasible model for loop J–K, which becomes unstructured when reorienting the CTD relative to the NTD. In our final model of OCP^r [which includes the translocated CTD and refined loop J–K (Figure 4D–F)], all of the amino acids implicated in cross-linking are in the proximity, within 30 Å. We must assume that for the flexible NTE, the meaningful structural constraints come from the K^{167}–K^{249} and K^{170}–K^{249} cross-links, the lengths of which are 12.7 and 18.7 Å, respectively. We admit that this modeling treatment is preliminary, and that the refined structure of loop J–K is entirely dependent on our proposed reorientation of the CTD relative to the NTD. Nevertheless, we consider this a useful first step for future structural refinements. Our model does not necessarily exclude other models in which the 12 Å cross-linker fails to conjugate. It is highly possible that loop J–K could allow multiple orientations of the NTD and CTD in solution, while *in vivo*, the PBS binding pocket could preferably select those OCP^r forms that are structurally available for interaction. The flexible NTE, with a length of 30.6 Å from P2 to D19, also presents a problem. If unfolding of αA is considered, the arm span of NTE could be even longer. At any rate, our experiment establishes the cross-linking network in OCP^r, allowing for structural refinement of OCP^r by other methods. This model assumes that the separation of the NTD and CTD as well as that of the CTD

DOI: 10.1021/acs.biochem.6b00013
Biochemistry 2016, 55, 1003–1009

does not impose any structural effect upon the binding of the NTD and carotenoid cofactor to PBS.

In summary, we successfully modified OCP^o and OCP^r and locked them in their characteristic states using isotopically coded cross-linkers. The spatial conflicts of cross-linking pairs uniquely detected in OCP^r compared to OCP^o support the idea that OCP undergoes dramatic conformational changes from the perspective of NTD and CTD orientation. On the basis of previously published results and our current results, we propose an updated intramolecular signal propagation pathway for OCP activation in conjunction with the carotenoid translation. Upon photon absorption, the pigment's effective conjugation length is increased, contributing to the breaking of the H-bonding network within OCP^r. The interactions of the major interface between the NTD and CTD and the minor interface between the NTE and CTD weaken and collapse upon translocation of the pigment toward the NTD. The NTD and CTD are completely detached and are then guided by an intrinsic structural cue from loop J−K, so that the PBS and FRP binding interfaces on OCP^r are exposed for PBS energy quenching and fluorescence recovery.

AUTHOR INFORMATION

Corresponding Author

*Washington University in St. Louis, One Brookings Drive, Campus Box 1137, St. Louis, MO 63130. Telephone: +1-314-935-7971. E-mail: blankenship@wustl.edu.

Funding

This research is funded by the U.S. Department of Energy (DOE), Office of Basic Energy Sciences (Grant DE-FG02-07ER15902 to R.E.B.). H.L. was funded by the DOE grant. J.D.K. was supported by a Monsanto Graduate Fellowship. Instrumentation was made available by the Photosynthetic Antenna Research Center (PARC), an Energy Frontier Research Center funded by the U.S. Department of Energy (DOE), Office of Basic Energy Sciences (Grant DE-SC0001035 to R.E.B.). J.J., G.S.O., and H.Z. were funded by the PARC grant. The research was also supported by the National Institute of General Medical Sciences (Grant 2P41 GM103422 to M.L.G.).

Notes

The authors declare no competing financial interest.

ACKNOWLEDGMENTS

The authors thank Prof. Robert Chalkley and Dr. Peter Baker from UCSF Mass Spectrometry Facility for help with Protein Prospector.

ABBREVIATIONS

OCP, orange carotenoid protein; NTD, N-terminal domain; CTD, C-terminal domain; LHC, light-harvesting complex; RC, reaction center; NADPH, nicotinamide adenine dinucleotide phosphate; NPQ, nonphotochemical quenching; PBS, phycobilisome; MW, molecular weight; OCP^o, orange form of OCP; OCP^r, red from of OCP; NTE, N-terminal extension; FRP, fluorescence recovery protein; FPLC, fast protein liquid chromatography; LysC, Lys-C protease; HCD, high-energy collision-induced dissociation; SDS−PAGE, sodium dodecyl sulfate−polyacrylamide gel electrophoresis; LC−MS/MS, liquid chromatography−tandem mass spectrometry; PDB, Protein Data Bank.

REFERENCES

(1) Blankenship, R. E. (2014) *Molecular Mechanisms of Photosynthesis*, Blackwell Science, Oxford, U.K.

(2) Umena, Y., Kawakami, K., Shen, J. R., and Kamiya, N. (2011) Crystal structure of oxygen-evolving photosystem II at a resolution of 1.9 A. *Nature 473*, 55−60.

(3) Jordan, P., Fromme, P., Witt, H. T., Klukas, O., Saenger, W., and Krauss, N. (2001) Three-dimensional structure of cyanobacterial photosystem I at 2.5 A resolution. *Nature 411*, 909−917.

(4) Niyogi, K. K., and Truong, T. B. (2013) Evolution of flexible non-photochemical quenching mechanisms that regulate light harvesting in oxygenic photosynthesis. *Curr. Opin. Plant Biol. 16*, 307−314.

(5) Horton, P., and Ruban, A. (2004) Molecular design of the photosystem II light-harvesting antenna: photosynthesis and photoprotection. *J. Exp Bot 56*, 365−373.

(6) Muller, P., Li, X. P., and Niyogi, K. K. (2001) Non-photochemical quenching. A response to excess light energy. *Plant Physiol. 125*, 1558−1566.

(7) Wilson, A., Ajlani, G., Verbavatz, J. M., Vass, I., Kerfeld, C. A., and Kirilovsky, D. (2006) A soluble carotenoid protein involved in phycobilisome-related energy dissipation in cyanobacteria. *Plant Cell 18*, 992−1007.

(8) Kirilovsky, D., and Kerfeld, C. A. (2012) The orange carotenoid protein in photoprotection of photosystem II in cyanobacteria. *Biochim. Biophys. Acta, Bioenerg. 1817*, 158−166.

(9) Kay Holt, T., and Krogmann, D. W. (1981) A Carotenoid-Protein from Cyanobacteria. *Biochim. Biophys. Acta, Bioenerg. 637*, 408−414.

(10) Kerfeld, C. A., Yoshida, S., Tran, K. T., Yeates, T. O., Cascio, D., Bottin, H., Berthomieu, C., Sugiura, M., and Boussac, A. (2003) The 1.6 A resolution structure of Fe-superoxide dismutase from the thermophilic cyanobacterium Thermosynechococcus elongatus. *JBIC, J. Biol. Inorg. Chem. 8*, 707−714.

(11) Wilson, A., Kinney, J. N., Zwart, P. H., Punginelli, C., D'Haene, S., Perreau, F., Klein, M. G., Kirilovsky, D., and Kerfeld, C. A. (2010) Structural determinants underlying photoprotection in the photoactive orange carotenoid protein of cyanobacteria. *J. Biol. Chem. 285*, 18364−18375.

(12) Kirilovsky, D., and Kerfeld, C. A. (2013) The Orange Carotenoid Protein: a blue-green light photoactive protein. *Photochem. Photobiol. Sci. 12*, 1135−1143.

(13) Gupta, S., Guttman, M., Leverenz, R. L., Zhumadilova, K., Pawlowski, E. G., Petzold, C. J., Lee, K. K., Ralston, C. Y., and Kerfeld, C. A. (2015) Local and global structural drivers for the photoactivation of the orange carotenoid protein. *Proc. Natl. Acad. Sci. U. S. A. 112*, E5567−5574.

(14) Liu, H., Zhang, H., King, J. D., Wolf, N. R., Prado, M., Gross, M. L., and Blankenship, R. E. (2014) Mass spectrometry footprinting reveals the structural rearrangements of cyanobacterial orange carotenoid protein upon light activation. *Biochim. Biophys. Acta, Bioenerg. 1837*, 1955−1963.

(15) Thurotte, A., Lopez-Igual, R., Wilson, A., Comolet, L., Bourcier de Carbon, C., Xiao, F., and Kirilovsky, D. (2015) Regulation of Orange Carotenoid Protein Activity in Cyanobacterial Photoprotection. *Plant Physiol. 169*, 737−747.

(16) Leverenz, R. L., Sutter, M., Wilson, A., Gupta, S., Thurotte, A., Bourcier de Carbon, C., Petzold, C. J., Ralston, C., Perreau, F., Kirilovsky, D., and Kerfeld, C. A. (2015) PHOTOSYNTHESIS. A 12 A carotenoid translocation in a photoswitch associated with cyanobacterial photoprotection. *Science 348*, 1463−1466.

(17) Boulay, C., Wilson, A., D'Haene, S., and Kirilovsky, D. (2010) Identification of a protein required for recovery of full antenna capacity in OCP-related photoprotective mechanism in cyanobacteria. *Proc. Natl. Acad. Sci. U. S. A. 107*, 11620−11625.

(18) Sutter, M., Wilson, A., Leverenz, R. L., Lopez-Igual, R., Thurotte, A., Salmeen, A. E., Kirilovsky, D., and Kerfeld, C. A. (2013) Crystal structure of the FRP and identification of the active site for modulation of OCP-mediated photoprotection in cyanobacteria. *Proc. Natl. Acad. Sci. U. S. A. 110*, 10022−10027.

DOI: 10.1021/acs.biochem.6b00013
Biochemistry 2016, 55, 1003−1009

(19) Gorbunov, M. Y., Kuzminov, F. I., Fadeev, V. V., Kim, J. D., and Falkowski, P. G. (2011) A kinetic model of non-photochemical quenching in cyanobacteria. *Biochim. Biophys. Acta, Bioenerg. 1807*, 1591−1599.
(20) Polivka, T., Kerfeld, C. A., Pascher, T., and Sundstrom, V. (2005) Spectroscopic properties of the carotenoid 3′-hydroxyechinenone in the orange carotenoid protein from the cyanobacterium Arthrospira maxima. *Biochemistry 44*, 3994−4003.
(21) Zhang, H., Liu, H., Niedzwiedzki, D. M., Prado, M., Jiang, J., Gross, M. L., and Blankenship, R. E. (2014) Molecular mechanism of photoactivation and structural location of the cyanobacterial orange carotenoid protein. *Biochemistry 53*, 13−19.
(22) Leverenz, R. L., Jallet, D., Li, M. D., Mathies, R. A., Kirilovsky, D., and Kerfeld, C. A. (2014) Structural and functional modularity of the orange carotenoid protein: distinct roles for the N- and C-terminal domains in cyanobacterial photoprotection. *Plant Cell 26*, 426−437.
(23) Kuzminov, F. I., Karapetyan, N. V., Rakhimberdieva, M. G., Elanskaya, I. V., Gorbunov, M. Y., and Fadeev, V. V. (2012) Investigation of OCP-triggered dissipation of excitation energy in PSI/PSII-less Synechocystis sp. PCC 6803 mutant using non-linear laser fluorimetry. *Biochim. Biophys. Acta, Bioenerg. 1817*, 1012−1021.
(24) Maksimov, E. G., Shirshin, E. A., Sluchanko, N. N., Zlenko, D. V., Parshina, E. Y., Tsoraev, G. V., Klementiev, K. E., Budylin, G. S., Schmitt, F. J., Friedrich, T., Fadeev, V. V., Paschenko, V. Z., and Rubin, A. B. (2015) The Signaling State of Orange Carotenoid Protein. *Biophys. J. 109*, 595−607.
(25) Wilson, A., Punginelli, C., Gall, A., Bonetti, C., Alexandre, M., Routaboul, J. M., Kerfeld, C. A., van Grondelle, R., Robert, B., Kennis, J. T., and Kirilovsky, D. (2008) A photoactive carotenoid protein acting as light intensity sensor. *Proc. Natl. Acad. Sci. U. S. A. 105*, 12075−12080.
(26) Kashino, Y., Koike, H., and Satoh, K. (2001) An improved sodium dodecyl sulfate-polyacrylamide gel electrophoresis system for the analysis of membrane protein complexes. *Electrophoresis 22*, 1004−1007.
(27) Leitner, A., Walzthoeni, T., and Aebersold, R. (2013) Lysine-specific chemical cross-linking of protein complexes and identification of cross-linking sites using LC-MS/MS and the xQuest/xProphet software pipeline. *Nat. Protoc. 9*, 120−137.
(28) Kessner, D., Chambers, M., Burke, R., Agus, D., and Mallick, P. (2008) ProteoWizard: open source software for rapid proteomics tools development. *Bioinformatics 24*, 2534−2536.
(29) Chambers, M. C., Maclean, B., Burke, R., Amodei, D., Ruderman, D. L., Neumann, S., Gatto, L., Fischer, B., Pratt, B., Egertson, J., Hoff, K., Kessner, D., Tasman, N., Shulman, N., Frewen, B., Baker, T. A., Brusniak, M. Y., Paulse, C., Creasy, D., Flashner, L., Kani, K., Moulding, C., Seymour, S. L., Nuwaysir, L. M., Lefebvre, B., Kuhlmann, F., Roark, J., Rainer, P., Detlev, S., Hemenway, T., Huhmer, A., Langridge, J., Connolly, B., Chadick, T., Holly, K., Eckels, J., Deutsch, E. W., Moritz, R. L., Katz, J. E., Agus, D. B., MacCoss, M., Tabb, D. L., and Mallick, P. (2012) A cross-platform toolkit for mass spectrometry and proteomics. *Nat. Biotechnol. 30*, 918−920.
(30) Chalkley, R. J., Trnka, M. J., Michael, N., and Baker, P. R. (2014) Identifying Cross-linked Peptides using Protein Prospector. 62nd ASMS Conference of Mass Spectrometry and Allied Topics, Baltimore, MD, June 15.
(31) Trnka, M. J., Baker, P. R., Robinson, P. J., Burlingame, A. L., and Chalkley, R. J. (2014) Matching cross-linked peptide spectra: only as good as the worse identification. *Mol. Cell. Proteomics 13*, 420−434.
(32) DeLano, W. L. (2002) *The PyMol Molecular Graphics System*, DeLano Scientific, Palo Alto, CA.
(33) Webb, B., and Sali, A. (2014) Comparative Protein Structure Modeling Using MODELLER. *Current protocols in bioinformatics 47*, 5.6.1−5.6.32.
(34) Webb, B., and Sali, A. (2014) Protein structure modeling with MODELLER. *Methods Mol. Biol. 1137*, 1−15.
(35) Sinz, A. (2014) The advancement of chemical cross-linking and mass spectrometry for structural proteomics: from single proteins to protein interaction networks. *Expert Rev. Proteomics 11*, 733−743.
(36) Bricker, T. M., Mummadisetti, M. P., and Frankel, L. K. (2015) Recent advances in the use of mass spectrometry to examine structure/function relationships in photosystem II. *J. Photochem. Photobiol., B 152*, 227−246.
(37) Bricker, T. M., Odom, W. R., and Queirolo, C. B. (1988) Close Association of the 33-Kda Extrinsic Protein with the Apoprotein of Cpa1 in Photosystem-Ii. *FEBS Lett. 231*, 111−117.
(38) Seidler, A. (1996) Intermolecular and intramolecular interactions of the 33-kDa protein in photosystem II. *Eur. J. Biochem. 242*, 485−490.
(39) Mummadisetti, M. P., Frankel, L. K., Bellamy, H. D., Sallans, L., Goettert, J. S., Brylinski, M., Limbach, P. A., and Bricker, T. M. (2014) Use of protein cross-linking and radiolytic footprinting to elucidate PsbP and PsbQ interactions within higher plant Photosystem II. *Proc. Natl. Acad. Sci. U. S. A. 111*, 16178−16183.
(40) Kerfeld, C. A., Sawaya, M. R., Brahmandam, V., Cascio, D., Ho, K. K., Trevithick-Sutton, C. C., Krogmann, D. W., and Yeates, T. O. (2003) The crystal structure of a cyanobacterial water-soluble carotenoid binding protein. *Structure 11*, 55−65.
(41) Zheng, C., Yang, L., Hoopmann, M. R., Eng, J. K., Tang, X., Weisbrod, C. R., and Bruce, J. E. (2011) Cross-linking measurements of in vivo protein complex topologies. *Mol. Cell. Proteomics 10*, M110.006841.
(42) Rappsilber, J. (2011) The beginning of a beautiful friendship: cross-linking/mass spectrometry and modelling of proteins and multi-protein complexes. *J. Struct. Biol. 173*, 530−540.
(43) Liu, H., Zhang, H., Weisz, D. A., Vidavsky, I., Gross, M. L., and Pakrasi, H. B. (2014) MS-based cross-linking analysis reveals the location of the PsbQ protein in cyanobacterial photosystem II. *Proc. Natl. Acad. Sci. U. S. A. 111*, 4638−4643.
(44) Tabb, D. L. (2012) Evaluating protein interactions through cross-linking mass spectrometry. *Nat. Methods 9*, 879−881.
(45) Rinner, O., Seebacher, J., Walzthoeni, T., Mueller, L. N., Beck, M., Schmidt, A., Mueller, M., and Aebersold, R. (2008) Identification of cross-linked peptides from large sequence databases. *Nat. Methods 5*, 315−318.
(46) Wilson, A., Punginelli, C., Couturier, M., Perreau, F., and Kirilovsky, D. (2011) Essential role of two tyrosines and two tryptophans on the photoprotection activity of the Orange Carotenoid Protein. *Biochim. Biophys. Acta, Bioenerg. 1807*, 293−301.
(47) Brodie, N. I., Makepeace, K. A., Petrotchenko, E. V., and Borchers, C. H. (2015) Isotopically-coded short-range hetero-bifunctional photo-reactive crosslinkers for studying protein structure. *J. Proteomics 118*, 12−20.

DOI: 10.1021/acs.biochem.6b00013
Biochemistry 2016, 55, 1003−1009